Interdisciplinary Research in Medical Sciences Specialty
ISSN: 3062-4401
2025, Volume 5, Issue 2, Page No: 233-253

Available online at: www.galaxypub.co/page/journals

Galaxy Publication

SHMT2-Driven Serine Metabolism Controls Membrane Phospholipid Remodeling and Cancer Stemness in Gastric Cancer

Mikko Lahtinen[1]*, Elina Salo[1], Juhani Virtanen[2]

[1]Department of Cancer Metabolism and Serine Biology, Faculty of Medicine, University of Helsinki, Helsinki, Finland.
[2]Department of Gastric Cancer Research and Stemness, Faculty of Medicine, University of Eastern Finland, Kuopio, Finland.

***E-mail** ✉ mikko.lahtinen@helsinki.fi

Received: 12 September 2025; **Revised:** 22 November 2025; **Accepted:** 25 November 2025

ABSTRACT

Cancer stem cells possess highly adaptable metabolic characteristics. Nonetheless, the precise mechanisms linking specific metabolic routes to the sustained stemness of gastric cancer cells are not well characterized. The present work identifies the critical contribution of serine hydroxymethyltransferase-2 (SHMT2) and serine to the functional interaction between one-carbon metabolism and lipid metabolism that supports stemness maintenance in gastric cancer. In clinical specimens, SHMT2 was strongly upregulated in both gastric cancer cells (GCs) and gastric cancer stem cells, with its expression levels closely associated with aggressive clinicopathological features and reduced survival in gastric cancer patients. From a mechanistic perspective, silencing SHMT2 lowered intracellular serine availability in the one-carbon pathway. This change subsequently reshaped the makeup and fluidity of membrane phospholipids, resulting in a marked decline in membrane lipid rafts. The consequent phospholipid reorganization prevented γ-secretase from localizing to lipid rafts, thereby blocking CD44 cleavage and the release of CD44-ICD. Consequently, CD44-ICD-mediated transcriptional activation of c-Myc and KLF4 was impaired, leading to the disruption of stemness properties in gastric cancer cells. Taken together, these observations reinforce the concept of metabolic flexibility in cancer stem cells and highlight the SHMT2/serine/lipid rafts signaling axis as a candidate biomarker for gastric cancer diagnosis and prognostic assessment. Moreover, we prepared HA-Exo-siSHMT2 nanoparticles to evaluate targeted therapeutic intervention in GC, thereby introducing a promising new direction for clinical gastric cancer management.

Keywords: CD44-ICD, Gastric cancer, Membrane phospholipid, Serine, SHMT2

How to Cite This Article: Lahtinen M, Salo E, Virtanen J. SHMT2-Driven Serine Metabolism Controls Membrane Phospholipid Remodeling and Cancer Stemness in Gastric Cancer. Interdiscip Res Med Sci Spec. 2025;5(2):233-53. https://doi.org/10.51847/GAN4mspFkV

Introduction

Gastric cancer (GC) represents one of the most aggressive malignancies worldwide and ranks as the third leading contributor to cancer mortality [1]. The disease is clinically notable for its propensity for metastasis and recurrence, phenomena largely driven by the self-renewal ability and persistent proliferation of gastric cancer stem cells (GCSCs). Elucidating the regulatory networks that sustain stemness in GC and identifying suitable molecular targets for therapy are therefore high priorities.

Cancer stem cells (CSCs) exert a profound influence on tumor biology through their distinctive metabolic reprogramming [2]. Unlike the majority of differentiated tumor cells that primarily utilize glycolysis, CSCs demonstrate considerable metabolic versatility, readily shifting between oxidative phosphorylation (OXPHOS), fatty acid metabolism, and other pathways in response to microenvironmental and nutritional conditions [3]. Under normoxic conditions, for instance, CSCs derive most of their energy from OXPHOS and fatty acid β-oxidation [4]. In hypoxic environments, they upregulate glycolytic enzymes and glucose transporters to enhance glycolysis [5]. Glutamine breakdown additionally supplies precursors for macromolecular synthesis and

glutathione production, while lipid metabolism is adjusted to preserve membrane structure. Such plasticity enables CSCs to thrive under fluctuating conditions. Our prior investigation uncovered aberrant one-carbon metabolism in GCSCs [6], suggesting its participation in stemness regulation. Nevertheless, the underlying molecular links between one-carbon metabolism and GCSC properties warrant deeper exploration.

Serine hydroxymethyltransferase-2 (SHMT2) serves as a central enzyme in one-carbon metabolism, catalyzing the bidirectional conversion of serine to glycine while supplying one-carbon units. These units are indispensable for the biosynthesis of nucleotides, proteins, and lipids that drive tumor expansion, and they further support the generation of glutathione and S-adenosylmethionine for redox control and epigenetic modulation [7]. SHMT2 activity also sustains formyl-methionyl-tRNA levels, which are required for mitochondrial protein synthesis initiation in several cancers, including those of the stomach, esophagus, and colorectum [8, 9]. Notably, restricting serine/glycine availability triggers the buildup of harmful lipid species, which suppresses spheroid formation and impedes tumor expansion [10]. These observations imply significant metabolic crosstalk between one-carbon and lipid pathways in CSCs. The current study therefore focused on determining how SHMT2-regulated serine/glycine metabolism influences GCSC stemness through lipid-related processes.

CD44 functions as an important transmembrane receptor that senses extracellular cues and converts them into intracellular signaling events, thereby promoting tumor progression. It is frequently overexpressed in cancer stem cells across multiple tumor types, such as colorectal, breast, and osteosarcoma [11]. Despite this association, the detailed pathways through which CD44 controls stemness remain incompletely defined. Microenvironmental stimuli are known to induce proteolytic cleavage of membrane CD44, releasing its extracellular domain (EXT) [12]. When positioned in lipid rafts, CD44 undergoes initial extracellular cleavage by matrix metalloproteinases (MMPs), followed by intramembrane processing of the remaining fragment by γ-secretase, which liberates the intracellular domain (ICD) [13]. Once released, CD44-ICD migrates to the nucleus and acts as a transcriptional co-regulator of CD44 itself and various oncogenes, thereby advancing tumorigenesis [14]. Elevated circulating CD44-ICD levels have been correlated with increased tumor burden, metastatic spread, and poorer clinical outcomes in gastric, colorectal, and breast cancers [15], underscoring its relevance to gastric cancer pathobiology.

Although RNA interference (RNAi) is a powerful tool for gene-specific silencing, its therapeutic utility depends on efficient and safe delivery vehicles for siRNA molecules [16]. Exosomes, naturally secreted vesicles involved in cell-to-cell communication, offer distinct advantages as carriers owing to their high biocompatibility, structural stability, and low immunogenicity [17]. They are capable of transporting diverse therapeutic payloads, including siRNAs, miRNAs, proteins, and small molecules [18]. Tumor-derived exosomes, in particular, can exploit their surface antigens for preferential homing to homologous cancer cells [19]. Building on these properties, we engineered GC-derived exosomes loaded with SHMT2 siRNA and surface-modified with hyaluronic acid (HA) to achieve targeted delivery in gastric cancer.

This investigation explored the significance of SHMT2-orchestrated communication between one-carbon metabolism and lipid metabolism in preserving stemness within GCSCs. We further constructed HA-modified exosomes delivering SHMT2 siRNA as a targeted therapeutic platform for GC. Reduction of SHMT2 led to serine depletion, which triggered phospholipid membrane reorganization and impaired CD44 processing in lipid rafts, thereby attenuating GCSC stemness. The developed HA-Exo-siSHMT2 formulation displayed favorable efficacy and safety profiles in GC models. These results introduce an innovative metabolic targeting strategy for the diagnosis and treatment of gastric cancer.

Materials and Methods

Cell culture, enrichment of gastric cancer stem cells, and reagents

GES-1 normal gastric epithelial cells along with the gastric cancer lines MKN-45, MGC-803, NUGC-3, and BGC-823 were acquired from the American Type Culture Collection. MGC-803 cells were propagated in Dulbecco's modified Eagle's medium containing 10% fetal bovine serum (FBS). The remaining lines (GES-1, MKN-45, NUGC-3, and BGC-823) were maintained in RPMI-1640 medium supplemented with 10% FBS. All cultures were incubated at 37 °C in a humidified environment supplied with 5% CO_2. For experiments involving serine withdrawal, GC cells were switched to serine-free medium (DM150110, Pricella) or kept in standard complete medium.

Gastric cancer stem cells (GCSCs) were isolated and expanded according to the method outlined in our previous publication [6]. Enrichment occurred in serum-free Dulbecco's modified Eagle's/F12 medium formulated with

0.4% bovine serum albumin (BSA; Sigma), 20 μL/mL B27 supplement (Invitrogen, USA), 20 ng/mL basic fibroblast growth factor (bFGF; Gibco), 10 ng/mL epidermal growth factor (Gibco), and 2 μg/mL heparin. Cultures were passaged every 7 days. Sphere formation efficiency was assessed as previously detailed, and the average volume of GCSC spheres was calculated based on measurements from 30 spheres.
Key reagents employed throughout the study included serine (L476400, Aladdin) and DSPE-PEG2000-HA (A66001, Ruisen Beier Bio-technology). Cy5-labeled siSHMT2 and plain siSHMT2 oligonucleotides were produced by GenePharma.

Patient tissue samples
Tissue microarrays (TMAs) of gastric cancer (TMA1, #ZL STC1602; TMA2, #ZL StmA961) containing 128 normal adjacent tissues (NATs) and 128 gastric carcinoma specimens were obtained from Shanghai WEIAO Biotech Company. Complete clinical records were available for 120 patients, who formed the basis for statistical analyses. No patient in this cohort had received nicotinamide treatment before surgery. Fresh GC tissues and matched NATs utilized for cholera toxin subunit B (CTB) lipid raft labeling were sourced from individuals who had not received prior radiotherapy or chemotherapy at the First Affiliated Hospital of Chongqing Medical University. All procedures were conducted with approval from the Ethics Committee of Chongqing Medical University.

Generation of stable SHMT2 knockdown cells using lentivirus
Lentiviral particles expressing short hairpin RNAs directed against SHMT2 (shSHMT2#1 and shSHMT2#2) or a control sequence (shNC) were supplied by GenePharma. Cells were transduced for 12 h and subsequently maintained under puromycin selection for 2 weeks to establish stable lines.

RNA extraction and real-time quantitative PCR
Total RNA was obtained from cultured cells with TRIzol reagent (Invitrogen). Reverse transcription was carried out using the PrimeScript RT Reagent Kit (TaKaRa). Real-time PCR amplification was performed with SYBR Premix Ex Taq II (TaKaRa). Relative transcript levels were quantified via the 2^−ΔCt^ method relative to an internal control.

Immunohistochemical staining
Immunohistochemistry was executed with the SP kit (PV-9000, Zsgb-bio). Tissue sections were baked at 60 °C overnight, deparaffinized, rehydrated, and subjected to antigen retrieval by heating in citrate buffer at 100 °C for 15 min. Following peroxidase blocking, primary antibodies specific for CD44, SHMT2, c-Myc, and KLF4 were applied overnight at 4 °C. After PBS rinses, secondary antibody incubation lasted 30 min. Visualization was achieved with DAB, followed by hematoxylin counterstaining as recommended by the manufacturer.
Staining was semi-quantitatively evaluated by an immunostaining score derived from multiplying staining intensity and the percentage of positively stained cells. Intensity was graded as 0 (none), 1 (weak), 2 (moderate), or 3 (strong). Proportion scores were assigned as 0 (0%), 1 (0–25%), 2 (26–50%), 3 (51–75%), or 4 (76–100%). Composite scores ranged from 0 to 12 [20, 21]. Scores ≤ 4 were defined as low expression, whereas scores > 4 were classified as high expression.

Immunofluorescence microscopy
Cells were fixed on glass slides with 4% paraformaldehyde for 15 min and blocked with BSA. Primary antibodies targeting CD44 and APH-1 were incubated overnight at 4 °C. Secondary antibodies (Alexa Fluor 647 goat anti-mouse IgG and Cy3 goat anti-rabbit IgG; Beyotime) were applied for 45 min at room temperature. Nuclei were visualized with DAPI staining for 5 min after PBS washing. Representative images were recorded using fluorescence and confocal laser scanning microscopy.

Detection and labeling of membrane lipid rafts
Membrane lipid rafts were stained using the Vybrant Alexa Fluor 555 Lipid Raft Labeling Kit (V34404; Invitrogen). Cells were labeled with fluorescent CTB conjugate for 10 min, followed by incubation with anti-CTB antibody at 4 °C for 15 min to induce crosslinking. After washing with chilled PBS, fixation was performed in

4% formaldehyde for 15 min at 4 °C. DAPI counterstaining was applied, and images were captured by confocal microscopy. Mean fluorescence intensity of labeled rafts was additionally quantified by flow cytometry.

Measurement of plasma membrane fluidity

Membrane fluidity was examined through fluorescence recovery after photobleaching (FRAP) experiments. Cells stained with DiI for 10 min at 37 °C were imaged on a Leica DMi8 microscope using LAS X software (Leica Microsystems). A pre-bleaching image was acquired, after which the region of interest was bleached with 80% laser intensity. Recovery of fluorescence was monitored at 2-second intervals for 2 minutes.

Complementary assessment was conducted with a commercial Membrane Fluidity Kit (Abcam, Cat# ab189819) per the manufacturer's guidelines. Fluorescence of 1-pyrenedecanoic acid (PDA) was excited at 350 nm, with emission intensities recorded at 400 nm (monomer form) and 460 nm (excimer form). Relative membrane fluidity was expressed as the excimer-to-monomer fluorescence ratio.

Chromatin immunoprecipitation (ChIP) assay

Chromatin immunoprecipitation was conducted utilizing a dedicated ChIP Kit (Thermo Fisher Scientific) together with antibodies specific for CD44 and isotype-matched IgG control.

Colony formation assay

Gastric cancer cells were seeded at a density of 1×10^3 cells per well into 6-well culture plates and allowed to grow under standard conditions. Following a 2-week incubation period, the resulting colonies were carefully washed, fixed with methanol for 15 min, and subsequently stained using 0.5% crystal violet solution for 5 min. Colonies were imaged and enumerated with the assistance of ImageJ software.

Cell invasion assay

The invasive potential of gastric cancer cells was determined via modified Boyden chamber experiments performed as previously outlined [22]. In short, MGC-803 (3×10^4), BGC-823 (6×10^4), and MKN-45 (6×10^4) cells suspended in 200 μL serum-free medium were placed onto the upper surface of 8 μm-pore Boyden chambers (Millipore) that had been coated with Matrigel at a 1:7.5 dilution (Millipore). The lower compartment was supplied with FBS-containing medium. After the appropriate incubation duration, cells that had penetrated the membrane were fixed and visualized by crystal violet staining in methanol. Each experiment was independently repeated three times.

Flow cytometry analysis

Cells were labeled with APC-conjugated anti-CD44 antibody (BD Biosciences, diluted 1:167) and PE-conjugated anti-CD133 antibody (BD Biosciences, diluted 1:50) through incubation at 4°C for 30 min. Following four washes with cold PBS, the cells were resuspended in PBS and the proportion of $CD44^+/CD133^+$ double-positive cells was quantified on a Beckman Coulter flow cytometer.

Western blot analysis

Both GC and GCSC populations were lysed in RIPA buffer supplemented with a protease and phosphatase inhibitor cocktail. Normalized protein lysates were resolved by sodium dodecyl sulfate-polyacrylamide gel electrophoresis (SDS-PAGE) and electrotransferred onto polyvinylidene fluoride membranes. Blots were incubated overnight at 4°C with primary antibodies of interest and then treated with the corresponding secondary antibody (Biosharp) for 1 h. Chemiluminescent detection was performed using Clarity Western ECL Substrate on a ChemiDoc XRS+ imaging station (Bio-Rad Laboratories). The primary antibodies employed were: SHMT2 (1:1000, 11099-1-AP; Proteintech), KLF4 (1:500, 1880-1-AP; Proteintech), c-Myc (1:1000, 10828-1-AP; Proteintech), CD44 (1:1000, ab97959; Abcam), β-Actin (1:1000, BA2305; BOSTER), Flotilin-1 (1:1000, ET7107-82; HUABIO), APH-1 (1:1000, WL05060; Wanlei Bio), PEN2 (1:1000, ET7109-26; HUABIO), Nicastrin (1:1000, ET7108-38; HUABIO), and Presenilin (1:1000, ET7109-26; HUABIO).

Lipid raft isolation

Isolation of lipid raft fractions was achieved with the UltraRIPA Kit for Lipid Raft (F015, BioDynamics Laboratory) following the supplier's recommended procedure. In brief, cells were harvested in 0.5 mL of solution

containing protease inhibitors, vortexed thoroughly, and kept on ice for 10 min. Centrifugation at 12,000 rpm for 10 min at 4°C separated the detergent-soluble non-raft fraction. The remaining detergent-resistant pellet was resuspended in 1 mL buffer A, vortexed, and centrifuged again under the same conditions, discarding the supernatant. Lipid raft proteins were then extracted by resuspending the pellet in 50 μL buffer B, vigorous vortexing for 5 min, room-temperature incubation for 5 min, and final centrifugation at 12,000 rpm for 10 min at 25°C. The supernatant representing the raft fraction was collected. Equal protein quantities from each fraction were analyzed by SDS-PAGE and immunoblotting. Raft components were further characterized by liquid chromatography-tandem mass spectrometry (LC-MS/MS; Shanghai Tbotree Biotech Company).

Metabolite analysis

GCSCs derived from control and SHMT2-knockdown MGC-803 lines were harvested and rapidly frozen in liquid nitrogen prior to metabolite extraction. Comprehensive metabolic profiling was conducted via LC-MS/MS according to established protocols. Raw spectral data were transformed into mzXML format using ProteoWizard (version 3.0.19282) and processed with XCMS software. Metabolite assignment relied on accurate mass measurements and fragmentation patterns matched against an internal MS/MS spectral library. The complete raw dataset is publicly accessible in the MetaboLights database under study identifier MTBLS12128.

Synthesis of HA-Exo-siSHMT2

Exosomes released by gastric cancer cells were prepared according to a previously published method [23]. These exosomes were loaded with siSHMT2 through ultrasonic treatment. A 1:1 mass ratio mixture of exosomes and siSHMT2 in PBS was sonicated at 20% amplitude using six 30 s pulses separated by 2 min cooling intervals. Subsequently, DSPE-PEG2000-HA was incorporated at a 20:1 weight ratio, and the suspension was incubated at 37°C for 48 h. Free ligands were eliminated by centrifugation at 3500 × g for 10 min.

Characterization of HA-Exo-siSHMT2

Morphological examination of HA-Exo-siSHMT2 nanoparticles was performed by transmission electron microscopy (TEM; Hitachi-7500). Hydrodynamic size and surface zeta potential were determined using a NanoBook Omni particle analyzer (Brookhaven Instrument Ltd.). Confocal laser scanning microscopy (CLSM) was employed to confirm the co-localization of Cy5-labeled siSHMT2 within PKH67-stained exosomes.

In vitro cellular uptake evaluation

Cellular internalization of HA-Exo-siSHMT2 was monitored by CLSM. MGC-803 cells (3×10^4 cells/dish) were plated in specialized CLSM dishes and cultured overnight. DiI-labeled HA-Exo-siSHMT2 was introduced in serum-free medium. At selected time points (1, 2, 3, and 4 h), cells were washed with PBS and fixed with paraformaldehyde. Nuclear staining was achieved with DAPI, after which uptake patterns were imaged by CLSM. Mammospheres derived from GCSCs were similarly examined by CLSM following 24 h exposure to HA-Exo-siSHMT2. Flow cytometric analysis was additionally performed to quantify uptake of DiI-labeled HA-Exo-siSHMT2 in MGC-803, MKN-45, and GES-1 cells after 1 h incubation.

Tumor formation and limiting dilution experiments

Limiting dilution assays in vivo were carried out with sphere-forming cells derived from genetically modified MGC-803/sh-SHMT2#2 and control MGC-803/shNC lines. Different numbers of MGC-803 cells (1×10^5, 1×10^4, and 1×10^3) were injected subcutaneously into 5-week-old nude mice, with seven animals per dosage group. The frequency of tumor-initiating cells was computed using extreme limiting dilution analysis software (http://bioinf.wehi.edu.au/software/elda/).

Tumorigenicity studies involved subcutaneous implantation of 1×10^6 stably transfected GC sphere-derived cells suspended in 100 μL PBS into 6-week-old BALB/c nude mice (n = 5 mice per group). Treatment groups received either no intervention or HA-Exo-siSHMT2 (20 μg administered every other day for 2 weeks). Mice were sacrificed on day 15, and tumors were collected. Tumor samples were processed either by paraffin embedding or immediate freezing in liquid nitrogen. Tumor size was determined according to the formula: volume = length × width² × 1/2. Excised tumors were analyzed by IHC for expression of SHMT2, CD44, c-Myc, and KLF4. Histological examination was also performed on sections stained with hematoxylin and eosin (HE).

For the orthotopic model, BALB/c nude mice were anesthetized using isoflurane inhalation. A small 1-cm incision was created in the abdominal wall under sterile conditions. GCSCs/MGC-803-Luc cells (1×10^6 cells in 100 μL sterile PBS) were inoculated directly into the stomach wall. The incision site was disinfected with iodine and closed using subcuticular sutures. Fifteen mice with established orthotopic tumors were randomly allocated to three groups (n = 5 per group): (1) PBS vehicle, (2) unmodified exosomes, and (3) HA-Exo-siSHMT2. Once tumors reached an appropriate volume, HA-Exo-siSHMT2 was given at a dose of 20 μg every 2 days over a 2-week period. Tumor burden was tracked non-invasively through bioluminescence imaging.
Ethics statement Animal studies received approval from the Institutional Animal Care and Use Committee of Chongqing Medical University (IACUC-CQMU-2024-04056). All procedures complied with the institutional guidelines on animal welfare at Chongqing Medical University.

Statistical analysis
Data analysis was performed with GraphPad Prism software (version 9.0). Patient survival was evaluated by the log-rank test. Comparisons between two experimental groups employed Student's t-test, whereas differences among multiple groups were assessed using one-way ANOVA. Statistical significance was defined as $p < 0.05$.

Results and Discussion

Elevated SHMT2 levels correlate with aggressive disease features, reduced patient survival, and enhanced stemness in gastric cancer
SHMT2 plays a prominent role in promoting tumor development and has attracted attention as a potential molecular target for cancer therapy. To explore its clinical relevance in gastric cancer, IHC staining was conducted on GC tissue microarrays to examine SHMT2 protein expression. Strong SHMT2 immunoreactivity was observed in malignant gastric tissues **(Figure 1a)**. Higher SHMT2 scores were significantly associated with advanced pT stage, lymph node metastasis, overall clinical stage, and poorer histological differentiation **(Figure 1b)**. Kaplan–Meier analysis of follow-up data from 80 patients indicated that those with elevated SHMT2 expression experienced markedly shorter survival times **(Figure 1c)**. Analysis of the TCGA database confirmed upregulated SHMT2 expression in tumor samples compared with normal gastric mucosa. Furthermore, high SHMT2 levels were linked to high-grade malignancies and inferior clinical prognosis. These results collectively highlight the connection between SHMT2 overexpression and the malignant phenotype of gastric cancer.

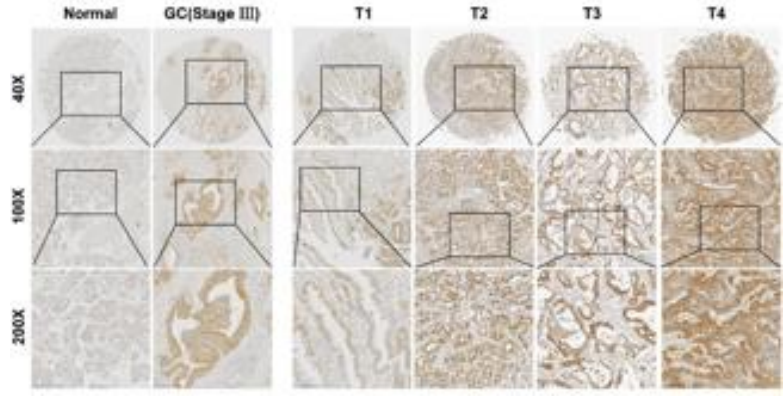

a)

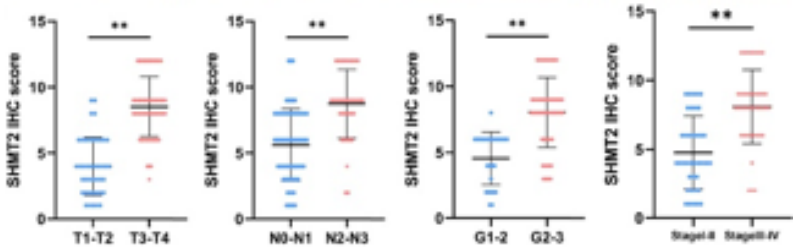

b)

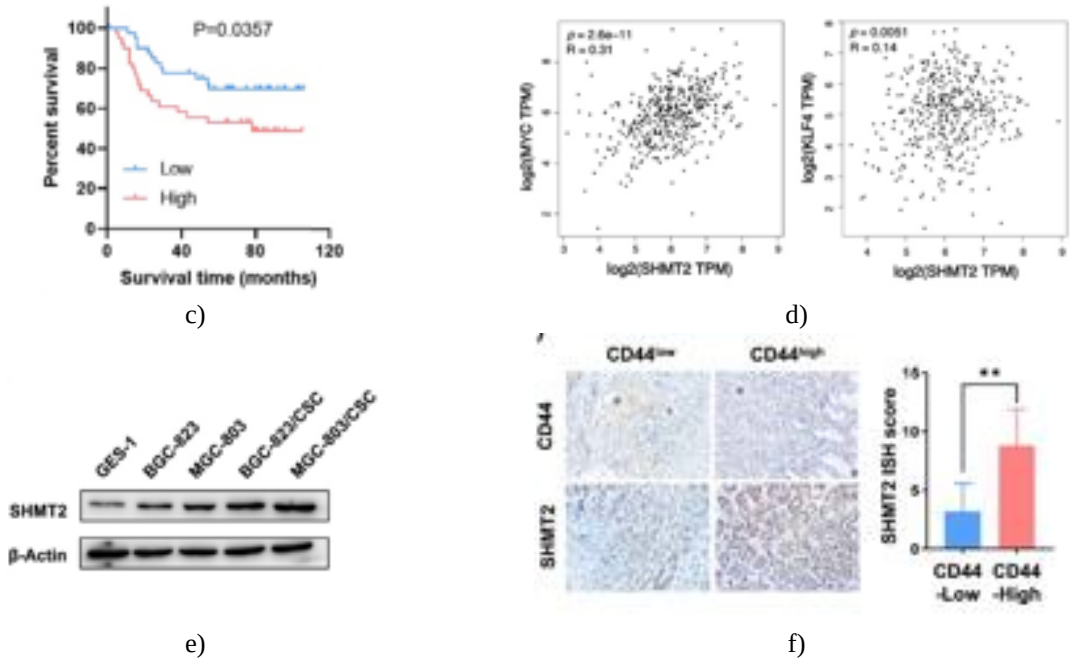

Figure 1. Increased SHMT2 abundance in gastric cancer tissues and stem cells is associated with unfavorable patient outcomes. (a) Typical immunohistochemical staining patterns of SHMT2 in 120 gastric cancer specimens. (b) Associations between SHMT2 IHC scores and tumor T stage, N stage, histological grade, and clinical stage ($p < 0.05$, $p < 0.01$). (c) Survival curves generated by the Kaplan–Meier method for gastric cancer patients stratified by high versus low SHMT2 expression according to IHC scoring of 80 cases ($p < 0.05$). (d) Western blot comparison of SHMT2 protein levels between GC cells and enriched GCSCs. (e) Correlation analysis of SHMT2 expression with stemness-related genes (MYC and KLF4) in the TCGA stomach adenocarcinoma (STAD) cohort. (f) Representative IHC images illustrating SHMT2 staining intensity in CD44-high versus CD44-low gastric cancer samples. Scale bar, 50 μm. Quantitative comparison of SHMT2 IHC scores between CD44-high and CD44-low groups ($p < 0.01$). CSC, cancer stem cell; GC, gastric cancer; GCSCs, gastric cancer stem cells; IHC, immunohistochemistry; SHMT2, serine hydroxymethyltransferase-2.

Our earlier investigation suggested that SHMT2 may contribute to the preservation of stem-like traits in gastric cancer stem cells [6]. To directly address this possibility, SHMT2 protein abundance was compared between parental GC cells and their stem cell derivatives, revealing substantially higher expression in the latter population **(Figure 1d)**. Application of the one-class logistic regression (OCLR) algorithm further demonstrated that patients exhibiting high SHMT2 expression possessed elevated stemness indices relative to those with low expression or healthy controls. Positive correlations were also detected between SHMT2 and the stemness transcription factors KLF4 and Myc **(Figure 1e)**. IHC examination confirmed that tumors with strong SHMT2 staining frequently displayed concurrent high levels of the stemness marker CD44 **(Figure 1f)**. In summary, these observations strongly support an intimate relationship between SHMT2 expression and the stemness program in gastric cancer.
Further experiments were performed to substantiate the importance of SHMT2 in preserving gastric cancer (GC) stemness. To this end, stable SHMT2-knockdown GC cell lines were established. These interventions resulted in a substantial reduction in cellular invasiveness **(Figures 2a and 2b)** and clonogenic potential **(Figures 2c and 2d)**. In addition, SHMT2-depleted GC stem cells (GCSCs) displayed impaired sphere-forming efficiency and smaller sphere sizes **(Figures 2e–2g)**. Levels of the stemness-related markers CD44, KLF4, and c-Myc were likewise significantly downregulated in the SHMT2-deficient GCSC spheres **(Figure 2h)**.
To evaluate the influence of SHMT2 on the tumorigenic capacity of GCSCs, sphere-derived cells were orthotopically implanted into nude mice. In vivo limiting dilution studies demonstrated that SHMT2 ablation markedly diminished tumor initiation rates **(Figure 2i)**. In line with these observations, SHMT2 knockdown also attenuated the growth of xenograft tumors **(Figure 2j)**. In reciprocal experiments, forced overexpression of SHMT2 in GES-1 (a normal gastric epithelial cell line) and NUGC-3 (a GC cell line expressing low levels of

SHMT2) cells robustly promoted invasive behavior, colony formation, and GCSC sphere generation, concomitant with upregulation of stemness markers. In summary, these findings establish that SHMT2 plays an indispensable role in supporting GCSC maintenance and self-renewal, thereby contributing to the malignant advancement of GC under both in vitro and in vivo conditions.

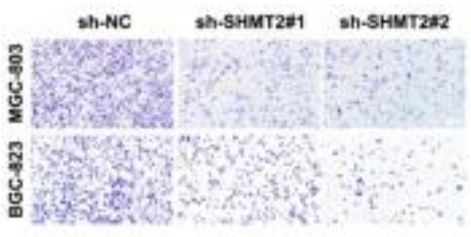

a)

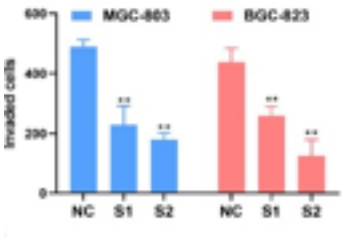

b)

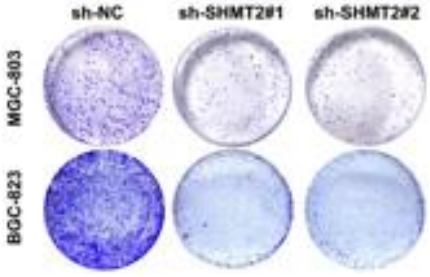

c)

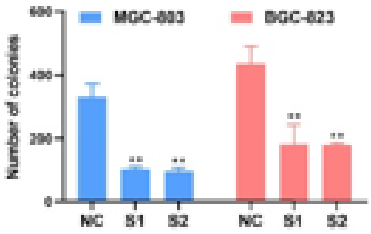

d)

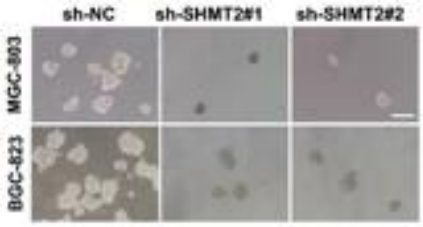

e)

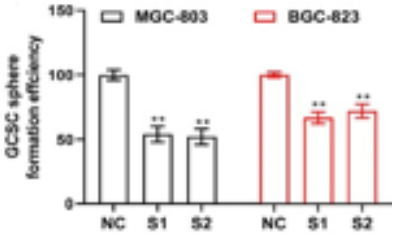

f)

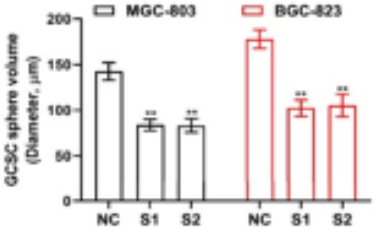

g)

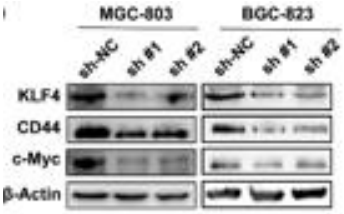

h)

Tumor size>0.1 cm³

Number of cells injected	shNC	sh SHMT2
10^3	2/7	0/7
10^4	4/7	2/7
10^5	7/7	5/7
Stem cell frequency (95% CI)	1/8704	1/65006
Fold change	7.47:1	
P-value	0.0009	

i)

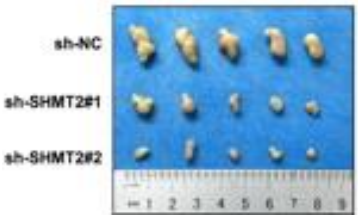

j)

Figure 2. Reduction of SHMT2 suppresses stem-like properties in gastric cancer stem cells. (a and b) Transwell assays illustrating decreased invasion of MGC-803 and BGC-823 cells upon SHMT2 knockdown (Scale bar, 100 μm, $p < 0.01$). (c and d) Quantification of colony formation in SHMT2-knockdown and control gastric cancer cells ($p < 0.01$). (e–g) Assessment of mammosphere formation ability. Representative sphere images, quantification of sphere numbers, and measurement of sphere volumes are displayed in panels (e–g), respectively ($p < 0.01$). Scale bar, 100 μm. (h) Immunoblot analysis of stemness proteins (c-Myc, KLF4, and CD44) in SHMT2-knockdown versus control cells. (i) Tumor-initiating frequency determined by

limiting dilution assay after subcutaneous injection of SHMT2-silenced MGC-803 CSCs (shSHMT2 #2) into BALB/c nude mice (n = 7 per group). (j) In vivo tumor growth curves showing reduced xenograft progression following SHMT2 knockdown. 1 × 10^6 sphere-derived MGC-803 cells (control or shSHMT2 #1/#2) were implanted subcutaneously. CSCs, cancer stem cells; GCSCs, gastric cancer stem cells; SHMT2, serine hydroxymethyltransferase-2.

SHMT2 plays a critical role in preserving the stemness properties of gastric cancer stem cells

SHMT2 functions as an essential enzyme mediating the metabolic interconversion of serine and glycine within the folate-dependent one-carbon metabolic network [24]. On this foundation, we proposed that SHMT2 likely supports tumor stemness maintenance by modulating serine/glycine availability. To test this premise, LC-MS/MS-based metabolomic profiling was conducted to evaluate serine and glycine dynamics in GCSCs following SHMT2 knockdown. The results demonstrated a pronounced reduction in serine abundance coupled with a reciprocal elevation in glycine content in SHMT2-depleted GCSCs relative to controls **(Figure 3a)**. These metabolic shifts imply that SHMT2 deficiency disrupts glycine-to-serine conversion in gastric cancer cells. Corroborating this observation, serum serine concentrations proved significantly elevated among GC patients compared with healthy controls, suggesting serine's contribution to GC pathogenesis.

To directly assess serine's requirement for GC stemness, GC cell lines were subjected to culture in serine-free conditions. Serine deprivation led to marked suppression of colony-forming potential, invasive capacity, and stemness marker protein expression in MGC-803, BGC-823, and MKN-45 cells compared with those maintained under standard nutrient conditions. These outcomes confirm that serine limitation attenuates stem-like properties in GC. Rescue experiments subsequently demonstrated that replenishing serine in SHMT2-knockdown GCSCs effectively reversed the impairment in stem cell sphere formation previously triggered by SHMT2 loss **(Figures 3b–3d)**. Analogous recovery patterns were observed in the abundance of CD44+CD133+ cells, a recognized CSC-enriched fraction in GC **(Figure 3e)**, as well as in colony formation and cell invasion after serine readdition. In keeping with these functional improvements, the downregulation of stemness-associated proteins induced by SHMT2 knockdown was largely restored by exogenous serine, particularly regarding KLF4, CD44, and c-Myc expression **(Figure 3f)**. Comparable restorative effects occurred in murine SHMT2-knockdown gastric cancer models upon serine supplementation. Collectively, the evidence indicates that high SHMT2 expression preserves GCSC stemness traits primarily by elevating intracellular serine levels.

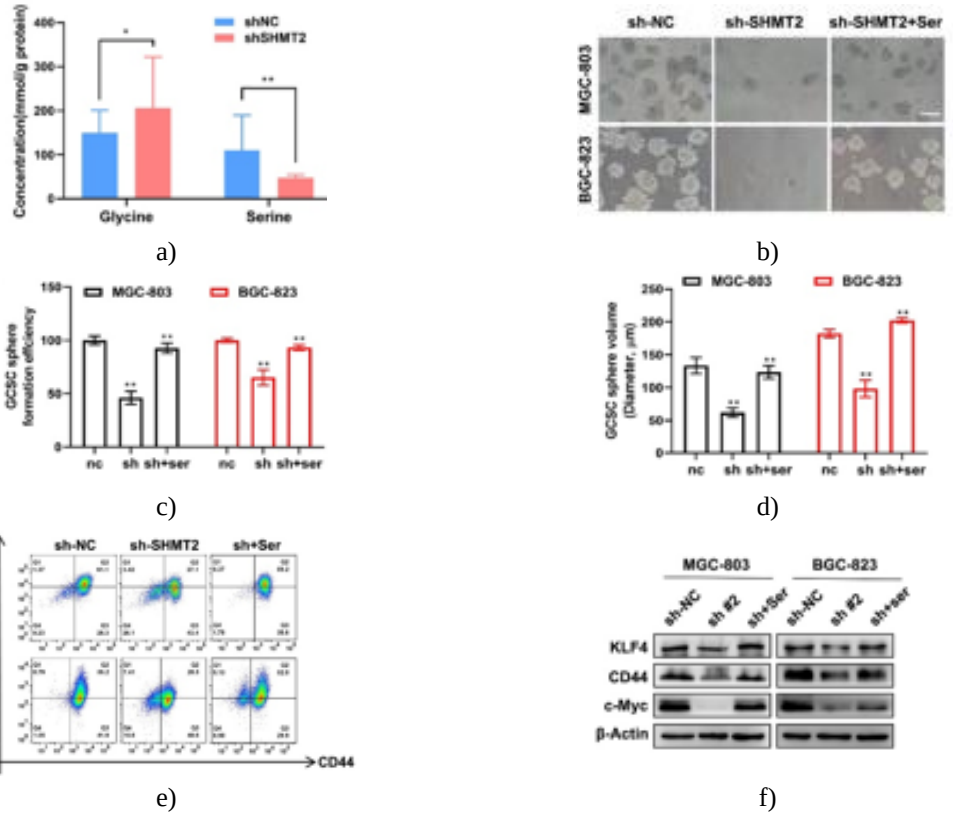

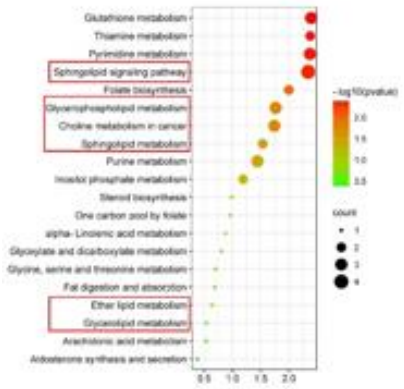

g)

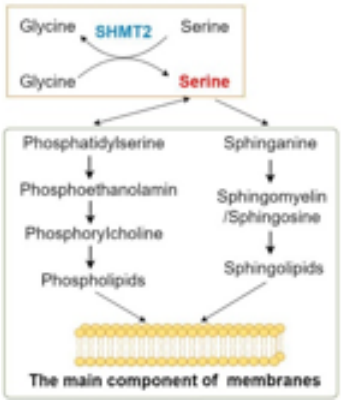

h)

Figure 3. SHMT2 depletion suppresses gastric cancer stemness via serine reduction. (a) Untargeted metabolomics revealing changes in serine and glycine concentrations in SHMT2-knockdown GCSCs versus controls ($p < 0.05$, $p < 0.01$). (b–d) Sphere formation rescue experiments in SHMT2-knockdown cells with or without serine addition. Representative images, sphere counts, and volumes are shown ($p < 0.01$). (e) Flow cytometry analysis of the $CD133^+/CD44^+$ CSC population. (f) Western blotting of stemness proteins in SHMT2-knockdown cells rescued with serine. (g) KEGG pathway enrichment from RNA-seq data of SHMT2-knockdown GCSCs. (h) Overview of metabolic connections between SHMT2 and serine. GCSCs, gastric cancer stem cells; SHMT2, serine hydroxymethyltransferase-2.

Deficiency in SHMT2 and serine triggers remodeling of membrane phospholipids, modifications in lipid profiles, and decreased membrane fluidity

To gain deeper insight into how SHMT2 modulates serine availability to support GCSC stemness, RNA sequencing was first performed for transcriptome-wide profiling of SHMT2-knockdown GCSCs. Subsequent KEGG pathway enrichment analysis highlighted prominent enrichment of lipid metabolism pathways in the SHMT2-depleted cells **(Figure 3g)**. In-depth inspection of one-carbon and lipid metabolic networks suggested that serine participates in the generation of major membrane phospholipids, including phosphatidylethanolamine (PE), phosphatidylcholine (PC), phosphatidylserine (PS), and sphingomyelin (SM) **(Figure 3h)**, notably through the base-exchange reactions facilitated by phosphatidylserine synthase 1 (PSS1) and phosphatidylserine synthase 2 (PSS2).

To establish whether SHMT2-dependent serine modulation drives lipid reprogramming in GCSCs, off-target lipid metabolomics was applied to profile lipid changes after SHMT2 knockdown. This approach identified widespread alterations in lipid metabolites within the knockdown cells **(Figure 4a)**, corroborating the pathway enrichment data. Detailed lipid composition assessment further uncovered significant reductions in key membrane phospholipid species such as SM, PE, and PC **(Figure 4b)**. Thus, SHMT2 deficiency appears to provoke extensive remodeling of lipid metabolism in GCSCs—particularly in membrane phospholipid pathways—through suppression of serine levels.

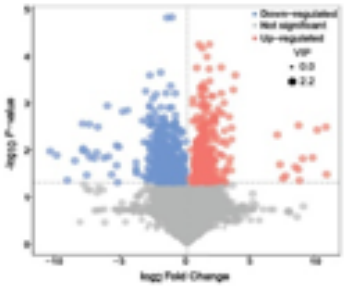

a)

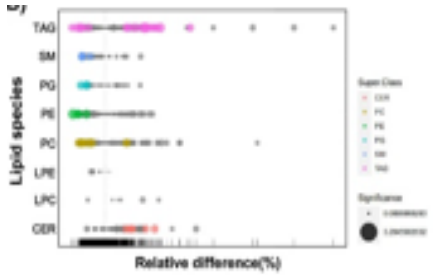

b)

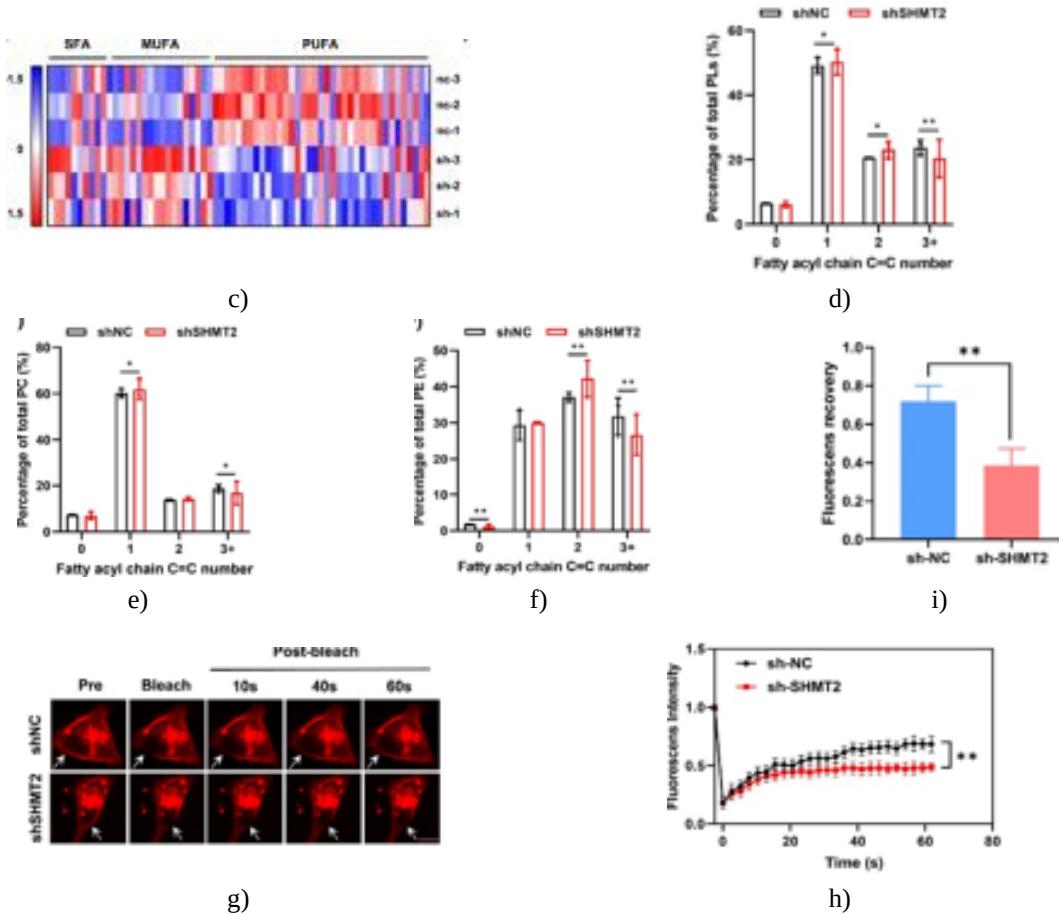

Figure 4. SHMT2 silencing decreases polyunsaturated fatty acid abundance and lowers membrane fluidity via serine downregulation. (a) Volcano plot illustrating changes in lipid metabolites between SHMT2 knockdown and control GCSCs. (b) Relative differences (%) in various lipids comparing SHMT2 knockdown versus control GCSCs. Individual dots represent distinct lipids; color reflects statistical significance and size corresponds to p value. (c) Heat map displaying variations in phospholipids containing saturated, monounsaturated, or polyunsaturated fatty acids. (d) Proportion of phospholipids exhibiting different saturation levels within total phospholipids (*p < 0.05, **p < 0.01). Saturation degree is defined by the number of carbon-carbon double bonds in fatty acyl chains. (e) Proportion of PCs with differing saturation levels among total PCs (*p < 0.05). (f) Proportion of PEs with differing saturation levels among total PEs (**p < 0.01). (g) Representative FRAP images from control and SHMT2-knockdown MGC-803 cells, with plasma membranes labeled by DiI (red fluorescence). (h) Fluorescence recovery curve demonstrating membrane recovery kinetics (**p < 0.01). (i) Quantitative FRAP recovery rate (post-bleach recovery relative to pre-bleach intensity) in SHMT2-knockdown MGC-803 cells versus controls (**p < 0.01). FRAP, fluorescence recovery after photobleaching; GC, gastric cancers; PCs, phosphatidylcholines; PEs, phosphatidylethanolamines; SHMT2, serine hydroxymethyltransferase-2.

Further scrutiny of the acyl chain distribution in phospholipids (PLs) from the SHMT2-knockdown lipidomic dataset revealed elevated proportions of saturated fatty acid-containing phospholipids (SFA-PLs) and monounsaturated fatty acid-containing phospholipids (MUFA-PLs), together with a substantial decline in polyunsaturated fatty acid-containing phospholipids (PUFA-PLs) **(Figure 4c)**. Evaluation of saturation status across PL classes confirmed reduced fractions of highly unsaturated species (≥3 double bonds) in total PLs **(Figure 4d)**, PCs **(Figure 4e)**, and PEs **(Figure 4f)** upon SHMT2 depletion. These shifts demonstrate that SHMT2 knockdown lowers PUFA incorporation in GCSCs. Given that phospholipid saturation and composition are known to govern membrane fluidity and functionality [25], the physical properties of cell membranes were next examined. Labeling with the phase-sensitive probe DiI (red fluorescence) followed by FRAP analysis showed markedly diminished membrane fluidity in SHMT2-deficient MGC-803 cells **(Figures 4g–4i)**. Parallel

experiments using a fluorescent PDA probe to gauge membrane viscosity in GC cells confirmed that SHMT2 loss reduces fluidity. These collective observations suggest that SHMT2/serine-regulated phospholipid metabolism plays a pivotal role in determining the lipid makeup and biophysical characteristics of the GC cell membrane.

SHMT2 and serine depletion decrease membrane lipid raft abundance and induce aberrant accumulation of CD44 within rafts

The composition and fluidity of membrane lipids are known to regulate the formation and stability of lipid rafts as well as the positioning and functional activity of raft-associated proteins [25]. Accordingly, we explored whether SHMT2 and serine status influence GC stemness by modulating the presence of stemness-related proteins in lipid raft microdomains. Initial experiments employed cholera toxin subunit B (CTB) staining to label ganglioside GM1, a classic lipid raft marker. This approach uncovered a substantial reduction in lipid raft density on the plasma membrane of GC cells upon SHMT2 knockdown **(Figure 5a)**. Notably, restoring serine levels in these SHMT2-deficient cells reversed the decline, as measured by flow cytometric quantification of CTB binding **(Figure 5b)**. In clinical specimens, lipid raft staining demonstrated significantly greater raft abundance in gastric carcinoma tissues than in matched paracancerous regions **(Figure 5c)**, supporting the potential involvement of lipid rafts in gastric tumor biology. Overall, these observations establish that SHMT2/serine deficiency lowers membrane lipid raft content as a consequence of altered membrane lipid organization.

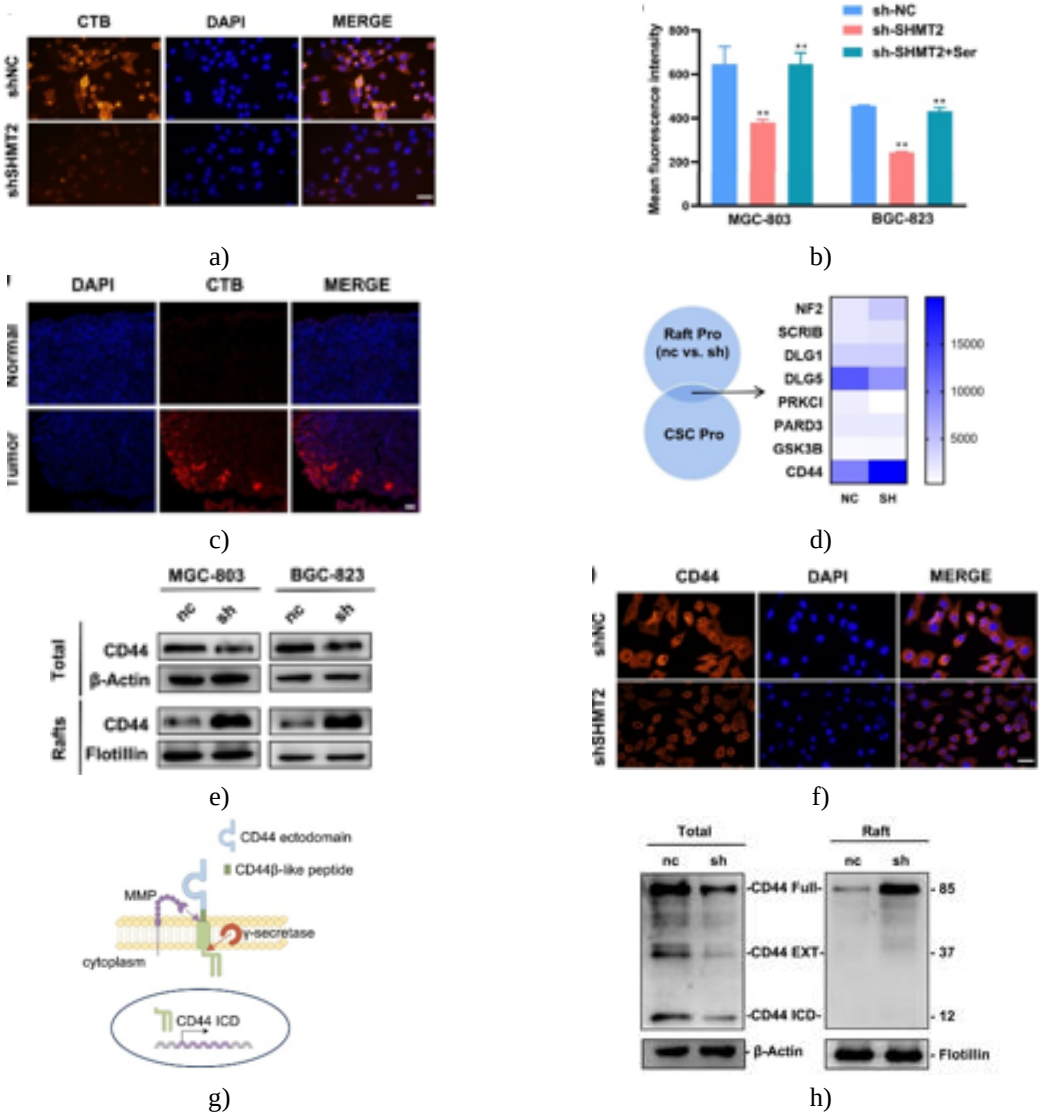

Figure 5. SHMT2/serine deficiency leads to reduced lipid raft levels and abnormal enrichment of CD44 in raft fractions. (a) Representative immunofluorescence images of lipid rafts (CTB-labeled, red) in control and

SHMT2 knockdown MGC-803 cells (Scale bar, 50 μm). (b) Flow cytometry-based quantification of mean fluorescence intensity for CTB-labeled lipid rafts in MGC-803 and BGC-823 cells following SHMT2 knockdown with or without serine supplementation (**p < 0.01). (c) Representative images of CTB-stained lipid rafts in gastric carcinoma versus adjacent normal tissues (Scale bar, 50 μm). (d) Venn diagram showing the intersection between cancer stemness proteins and differentially expressed proteins in SHMT2 knockdown versus control MGC-803 cells (left panel). Heatmap depicting expression patterns of the overlapping proteins (right panel). (e) Western blot detection of CD44 protein abundance in whole-cell lysates (Total) and isolated lipid raft fractions (Rafts) prepared from control and SHMT2 knockdown GC cells. Flotillin-1 was employed as a raft marker and β-actin as a loading control for total lysates. (f) Immunofluorescence analysis of CD44 subcellular localization in control and SHMT2 knockdown MGC-803 cells (Scale bar, 50 μm). (g) Schematic illustration depicting CD44 proteolytic processing within lipid rafts. (h) Levels of different CD44 cleavage products detected in total lysates and lipid raft fractions from control and SHMT2 knockdown MGC-803 cells. CTB, cholera toxin subunit B; GC, gastric cancer; SHMT2, serine hydroxymethyltransferase-2.

To delineate the impact of SHMT2 on membrane protein dynamics within lipid rafts, raft fractions were purified from both control and SHMT2-deficient MGC-803 cells. Proteomic profiling uncovered proteins differentially expressed in rafts that overlapped with stemness-associated candidates, among which CD44 exhibited prominent enrichment **(Figure 5d)**. Subsequent Western blot confirmation showed decreased overall CD44 protein in SHMT2-knockdown cells; however, the protein displayed strong accumulation specifically within the isolated raft fractions **(Figure 5e)**. Complementary immunofluorescence imaging indicated disrupted CD44 distribution, with the protein becoming predominantly confined to the plasma membrane following SHMT2 depletion **(Figure 5f)**. These results collectively suggest that SHMT2/serine deficiency, by remodeling membrane lipid architecture, promotes mislocalization of key membrane proteins into lipid rafts, most notably causing aberrant accumulation of the critical stemness factor CD44 in these domains.

Lack of γ-secretase localization in lipid rafts causes defective CD44 processing and diminished CD44 ICD release, thereby suppressing gastric cancer stemness properties

It has been established that CD44 positioned in lipid rafts undergoes proteolytic processing by γ-secretase, which liberates its intracellular domain (CD44-ICD). This liberated domain migrates into the nucleus and operates as a transcriptional regulator, driving the activation of oncogenes and contributing to tumor advancement **(Figure 5g)**. Accordingly, we proposed that the irregular distribution and buildup of CD44 within lipid rafts stemmed from impaired proteolytic processing. Initial experiments in MGC-803 cells with SHMT2 depletion revealed disruptions in CD44 processing, evidenced by lowered levels of both the extracellular domain (EXT) and intracellular domain (ICD) cleavage products **(Figure 5h)**, (left panel). In line with this, uncleaved CD44 showed anomalous enrichment in lipid rafts of SHMT2-depleted gastric cancer cells **(Figure 5h)**, (right panel).

To determine if these processing defects originated from mislocalization of γ-secretase within lipid rafts, we quantified the γ-secretase complex subunits (Presenilin, Nicastrin, PEN2, and APH-1) in whole-cell lysates and isolated raft fractions, alongside total CD44 ICD abundance. Overall cellular amounts of the individual subunits showed little variation; however, incorporation of the Nicastrin/APH-1 subcomplex into lipid rafts declined substantially upon SHMT2 silencing **(Figure 6a)**. Replenishment with serine reversed this reduction in raft-associated Nicastrin/APH-1 and concurrently restored CD44 ICD levels in total lysates **(Figure 6a)**. Parallel immunofluorescence studies confirmed that SHMT2 knockdown lowered lipid raft abundance and membrane APH-1 signals, phenotypes that were normalized following serine supplementation **(Figure 6b)**. Collectively, these observations underscore the requirement of intact lipid raft architecture for proper γ-secretase-dependent cleavage of CD44 to yield the ICD fragment.

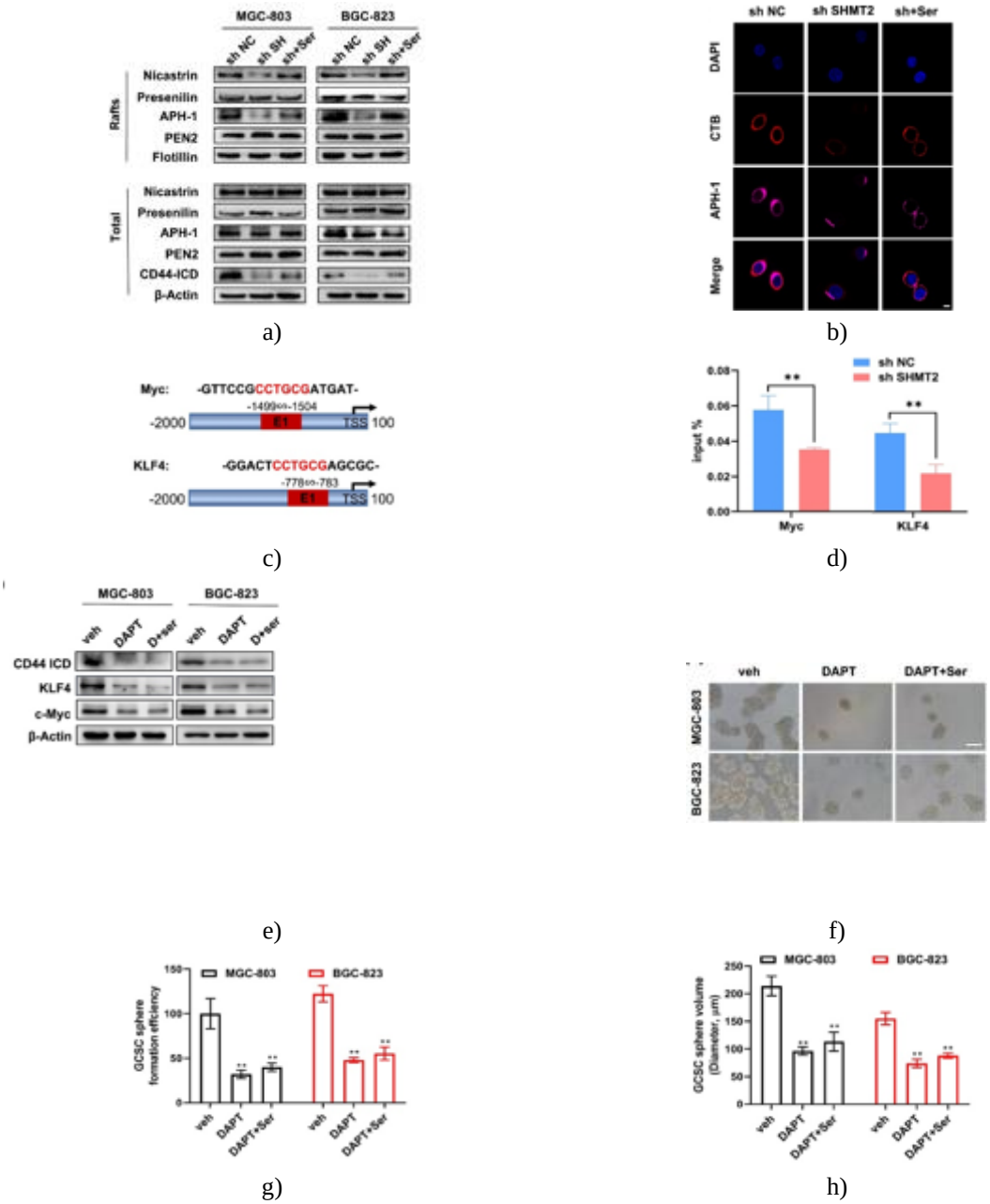

Figure 6. Deficient γ-secretase presence in lipid rafts induces faulty CD44 cleavage and limits CD44 ICD generation, leading to inhibition of gastric cancer stemness. (a) Western blot detection of γ-secretase subunits (Presenilin, Nicastrin, PEN2, and APH-1) together with CD44 ICD in total cell lysates (Total) and lipid raft fractions (Rafts) derived from SHMT2-knockdown cells, serine-rescued SHMT2-knockdown cells, and control gastric cancer cells. (b) Representative immunofluorescence micrographs depicting lipid rafts and APH-1 distribution in SHMT2-knockdown cells, serine-treated SHMT2-knockdown cells, and controls. Scale bar, 5 μm. (c) Identified binding motifs and locations of CD44 ICD interaction with the Myc and KLF4 promoter regions. (d) ChIP analysis illustrating CD44 ICD enrichment at the Myc and KLF4 promoters in SHMT2-knockdown versus control MGC-803 cells. (e) Western blot evaluation of CD44 ICD, c-Myc, and KLF4 protein levels after exposure to the γ-secretase inhibitor DAPT, with or without concurrent serine addition. (f–h) Evaluation of mammosphere-forming potential in cells treated with DAPT alone or combined with serine. Panels display representative sphere images, sphere counts, and sphere volumes, respectively (**p < 0.01**). GC, gastric cancer; ICD, intracellular domain; SHMT2, serine hydroxymethyltransferase-2.

Since prior work has identified CD44-ICD as a transcriptional activator recognizing the consensus motif CCTGCG [13], we explored its capacity to directly control the stemness regulators c-Myc and KLF4. Luciferase-based promoter assays validated the transcriptional influence of CD44 ICD on both Myc and KLF4. Sequence

inspection pinpointed the CD44 ICD interaction sites within the Myc and KLF4 promoters **(Figure 6c)**. Subsequent ChIP experiments demonstrated markedly lower CD44-ICD promoter occupancy at these loci in SHMT2-deficient gastric cancer cells **(Figure 6d)**, highlighting the necessity of CD44 ICD generation for sustaining c-Myc and KLF4 expression. Pharmacological blockade of γ-secretase with DAPT similarly suppressed c-Myc, KLF4, and CD44 ICD protein levels, and serine co-treatment failed to reverse these effects **(Figure 6e)**. Sphere-formation assays in gastric cancer stem cells mirrored this pattern **(Figures 6f–6h)**.
In summary, SHMT2 knockdown lowers intracellular serine availability, which perturbs membrane phospholipid profiles and reduces membrane fluidity. These changes compromise lipid raft stability, restrict γ-secretase recruitment to rafts, impair CD44 proteolytic release of the ICD, attenuate c-Myc and KLF4 expression, and ultimately compromise the self-renewal capacity of gastric cancer stem cells.

Efficiently engineered HA-exo-siSHMT2 suppresses gastric cancer stemness traits both in vitro and in vivo
Given the pivotal function of SHMT2 in preserving tumor stemness, we engineered a targeted delivery system using gastric cancer cell-derived exosomes carrying SHMT2-specific siRNA and modified with hyaluronic acid (HA), which serves as an effective ligand for CD44-overexpressing GCSCs. The HA-functionalized bovine exosomes loaded with SHMT2 siRNA (HA-Exo-siSHMT2) were generated according to the workflow depicted in **Figure 7a**. Particle morphology was visualized via transmission electron microscopy **(Figure 7b)**, (inset). Dynamic light scattering (DLS) characterization revealed an average hydrodynamic diameter of 162.8 ± 9.3 nm for HA-Exo-siSHMT2 **(Figure 7b)**. Zeta potential measurements yielded values of −35.24 ± 2.17 mV for the HA-modified exosomes and −30.56 ± 1.1 mV for unmodified exosomes **(Figure 7c)**. This negative surface charge facilitates better dispersion, minimizes aggregation in vivo, extends blood circulation half-life, and supports enhanced delivery performance. Storage stability assessments confirmed that HA-Exo-siSHMT2 retained consistent particle properties after being kept at −20°C for seven days **(Figure 7d)**.
Immunoblotting verified the retention of canonical exosome markers ALIX and HSP70 in both plain exosomes and HA-Exo-siSHMT2 constructs **(Figure 7e)**. HA was exclusively present in the modified preparations **(Figure 7e)**, confirming successful surface decoration. CLSM imaging displayed clear overlap between PKH67-stained exosomal membranes and Cy5-labeled SHMT2 siRNA **(Figure 7f)**, verifying efficient cargo incorporation. Overall, these analyses established the successful production of stable HA-Exo-siSHMT2 nanoparticles.

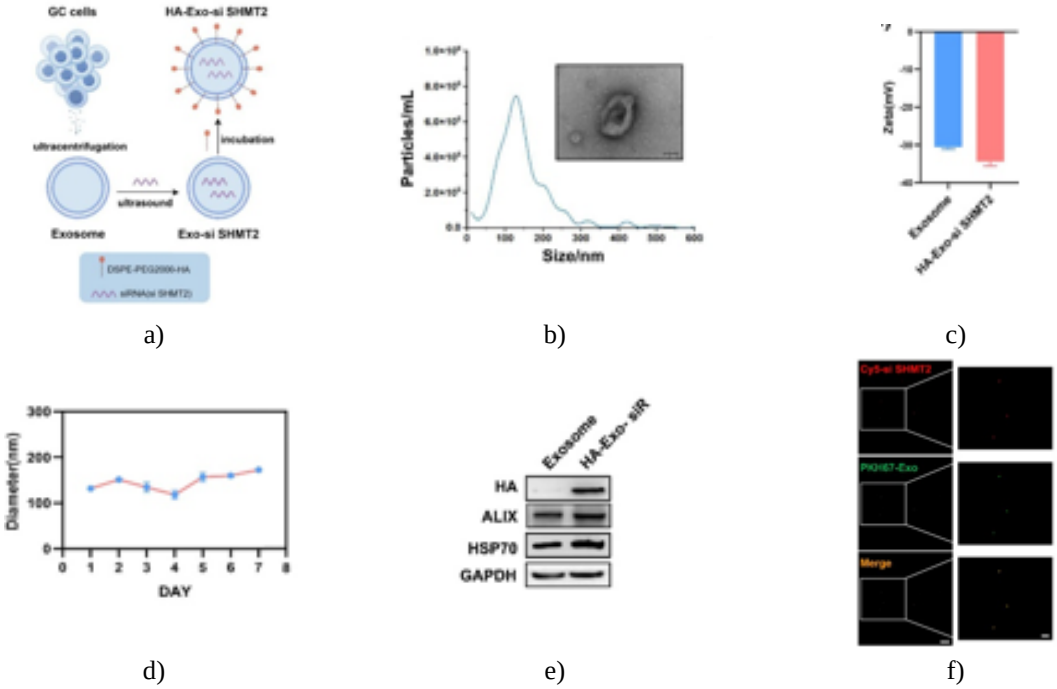

a) b) c)

d) e) f)

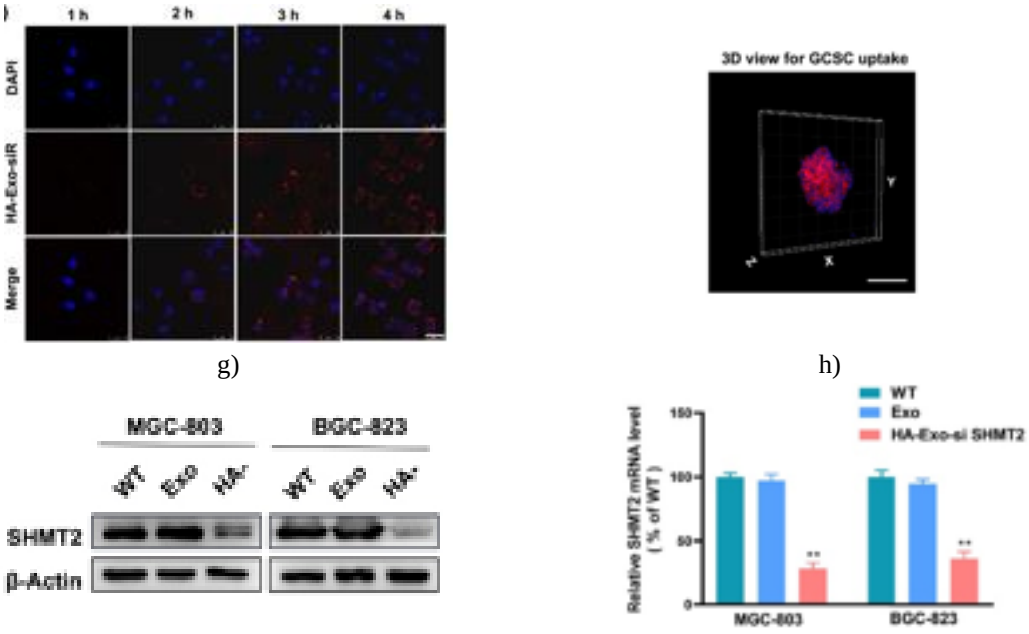

Figure 7. Fabrication and physicochemical characterization of HA-Exo-siSHMT2 particles, together with evaluation of their uptake by gastric cancer cells and gastric cancer stem cells. (a) Schematic representation outlining the assembly procedure for HA-Exo-siSHMT2. (b) Size distribution profile of HA-Exo-siSHMT2 obtained through DLS measurement. The inset shows a TEM micrograph of the nanoparticles. Scale bar: 50 nm. (c) Surface charge (zeta potential) profiles of native exosomes and HA-Exo-siSHMT2 as determined by DLS. (d) Changes in hydrodynamic size of HA-Exo-siSHMT2 monitored across a seven-day storage period. (e) Western blot detection of HA, ALIX, and HSP70 in native exosomes versus HA-Exo-siSHMT2. (f) CLSM micrographs demonstrating co-localization of Cy5-tagged SHMT2 siRNA within PKH67-labeled exosomes. Scale bars, 20 μm (left) and 5 μm (right). (g) Time-dependent internalization of HA-Exo-siSHMT2 in MGC-803 cells visualized by CLSM (scale bar = 50 μm). (h) CLSM images of HA-Exo-siSHMT2 uptake in MGC-803-derived GCSCs (scale bar = 100 μm). (I and J) Assessment of SHMT2 levels in GCs by western blot (i) and qRT-PCR (j) following treatment with HA-Exo-siSHMT2 (**p < 0.01**). GC, gastric cancer; GCSCs, gastric cancer stem cells; SHMT2, serine hydroxymethyltransferase-2.

Before advancing to therapeutic applications, the intracellular delivery efficiency of HA-Exo-siSHMT2 into GCs and GCSCs was thoroughly evaluated. DiI-labeled nanoparticles were incubated with target cells, and uptake dynamics were tracked using CLSM. Distinct cytoplasmic red fluorescence appeared in GCs within 1 h of exposure **(Figure 7g)**, with progressive intensification over time, indicating rapid and efficient internalization. In GCSC mammospheres, strong red signals were distributed throughout the structures after 24 h incubation **(Figure 7h)**, and three-dimensional reconstructions verified deep nanoparticle penetration. Notably, malignant MGC-803 and MKN-45 cells exhibited substantially greater uptake compared with non-malignant GES-1 cells, highlighting selective targeting toward transformed cells. Consistent with this, both qRT-PCR and western blot results confirmed robust downregulation of SHMT2 expression in treated GCs and GCSCs **(Figures 7l and 7j)**.
Subsequent functional assays validated the anti-stemness activity of HA-Exo-siSHMT2 in gastric cancer models. Exposure of MGC-803 and BGC-823 cells to the engineered exosomes led to pronounced inhibition of invasive behavior **(Figure 8a)**, decreased clonogenic potential **(Figure 8b)**, and marked reductions in both the number and volume of GCSC-derived spheres **(Figure 8c)**. Analogous suppression was recorded in MKN-45 cells. At the molecular level, treatment significantly lowered the abundance of CD44 ICD as well as the stemness transcription factors c-Myc and KLF4 in GCSCs **(Figure 8d)**. These data demonstrate that HA-Exo-siSHMT2 potently disrupts stem-like properties of gastric cancer cells in culture.

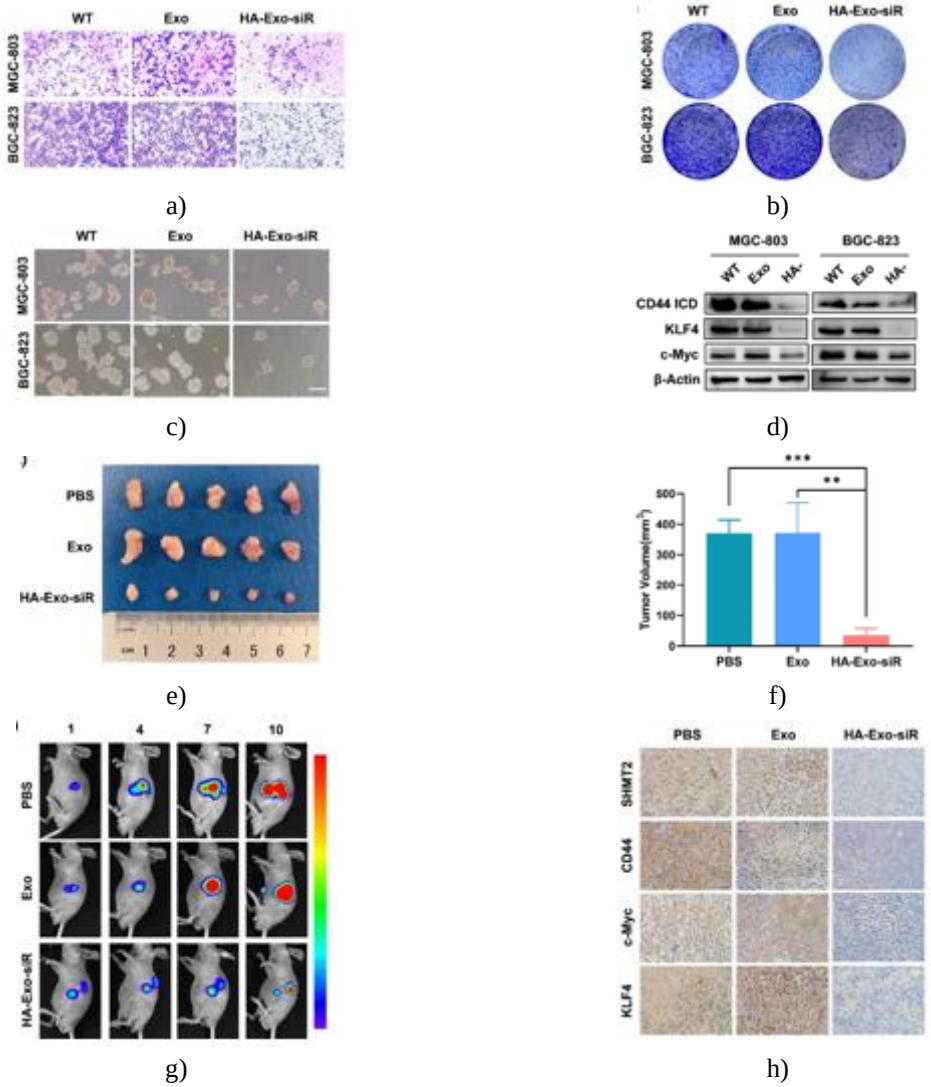

Figure 8. Evaluation of the therapeutic impact of HA-Exo-siSHMT2 in cell culture and animal models. (a) Assessment of GC cell invasive potential using Transwell chambers for wild-type (WT), unmodified exosome-treated, and HA-Exo-siSHMT2-treated conditions (scale bar, 100 μm). (b) Typical colony formation images of MGC-803 and BGC-823 GC cells under WT, exosome-treated, and HA-Exo-siSHMT2-treated conditions. (c) Characteristic mammosphere morphology observed in GC cells from the WT, exosome-treated, and HA-Exo-siSHMT2-treated groups. (d) Immunoblot analysis revealing expression levels of CD44 ICD, KLF4, and c-Myc proteins across the WT, exosome-treated, and HA-Exo-siSHMT2-treated groups. (e) Representative macroscopic images of tumors removed from mice in the untreated, exosome-treated, and HA-Exo-siSHMT2-treated experimental arms. (f) Growth curves showing subcutaneous tumor volumes in gastric cancer-bearing mice across untreated, exosome-treated, and HA-Exo-siSHMT2-treated cohorts. (g) In vivo bioluminescence imaging of orthotopic gastric tumors in nude mice recorded on days 1, 4, 7, and 10 after initiation of HA-Exo-siSHMT2 therapy. Scale bar: 2.000e+4–2.000e+5 p/s/cm²/sr. (h) Immunohistochemical staining for SHMT2, CD44, c-Myc, and KLF4 in subcutaneous tumor sections derived from untreated, exosome-treated, and HA-Exo-siSHMT2-treated animals (scale bar = 20 μm). GC, gastric cancer; ICD, intracellular domain; IHC, immunohistochemistry; SHMT2, serine hydroxymethyltransferase-2.

In the final set of experiments, the in vivo antitumor efficacy of HA-Exo-siSHMT2 was investigated in gastric cancer models. Systemic delivery through tail vein injection in mice bearing subcutaneous tumors resulted in a clear and statistically meaningful shrinkage of tumor burden after two weeks **(Figures 8e and 8f)**. Parallel studies in an orthotopic implantation model yielded similar outcomes, with live imaging confirming reduced tumor signals following HA-Exo-siSHMT2 administration **(Figure 8g)**. IHC staining of tumor tissues further demonstrated lowered abundance of key stemness regulators, including SHMT2, CD44, c-Myc, and KLF4, in the

treated group **(Figure 8h)**. Overall, these data highlight the ability of HA-Exo-siSHMT2 to effectively curb stem-like properties and limit tumor expansion in whole-animal systems.

Biosafety profiling involved histopathological review of major organs harvested from HA-Exo-siSHMT2-treated, exosome control, and untreated animals using HE staining. No overt pathological changes were detected in cardiac, hepatic, splenic, pulmonary, or renal tissues in either model, supporting a favorable safety margin. Consistent with this, routine blood chemistry panels displayed no meaningful deviations in key biochemical markers after nanoparticle exposure. In conclusion, HA-Exo-siSHMT2 exhibits strong biocompatibility and therapeutic promise, successfully diminishing gastric cancer stemness and impeding disease progression across both laboratory and living model contexts.

Owing to their unique metabolic adaptations, cancer stem cells occupy a central position in tumor initiation and progression. Consequently, detailed exploration of the metabolic traits of gastric cancer stem cells and their contribution to stemness preservation holds substantial importance for improving clinical diagnosis and treatment strategies in gastric cancer. The present study demonstrates that upregulated SHMT2 sustains GCSC stemness through its regulation of serine-glycine interconversion within one-carbon metabolism. This activity induces remodeling of membrane phospholipids, which in turn perturbs CD44 processing and localization within lipid rafts. In addition, we engineered HA-Exo-siSHMT2 as a targeted therapeutic platform directed against GC and GCSCs, thereby introducing a promising new avenue for clinical intervention in gastric cancer.

Cancer stem cells display considerable metabolic flexibility, enabling dynamic interactions among diverse pathways to meet demands for energy production, biomass synthesis, and redox balance. One-carbon metabolism constitutes a vital hub within this network, intersecting with amino acid metabolism, folate cycling, methionine metabolism, and the transsulfuration route. Recent evidence has linked the key one-carbon enzyme SHMT2 to lipid metabolic regulation, as illustrated by its control of hepatocyte lipid homeostasis through glycine-dependent mTOR signaling [26]. In agreement with such observations, our lipidomic profiling of SHMT2-knockdown GCSCs uncovered widespread changes across multiple lipid pathways, reinforcing the notion that SHMT2 bridges one-carbon and lipid metabolism.

SHMT2 catalyzes the reversible conversion of serine and glycine, a fundamental reaction in one-carbon metabolism. Earlier studies predominantly described net flux toward serine utilization, yet more recent work has highlighted a preference for glycine-to-serine conversion by mitochondrial SHMT2 [24, 27]. Consistent with the latter, SHMT2 depletion in GCSCs resulted in glycine accumulation and serine depletion, confirming the directionality of this reaction. Previous investigations have shown that serine limitation promotes toxic lipid metabolite buildup and restricts sphere formation and tumor expansion [9]. Our findings extend this knowledge by revealing that SHMT2 loss reduces serine availability, which disrupts GCSC stemness through membrane phospholipid remodeling and thereby provides fresh insight into metabolic crosstalk within these cells.

The lipid environment of the plasma membrane exerts precise control over membrane protein localization, stability, and signaling activity, particularly within lipid rafts. For example, LPCAT1-driven phospholipid saturation helps maintain EGFRvIII localization in lipid rafts of cancer cells [28]. In metastatic lung cancer, elevated SQS increases membrane cholesterol, enriching TNFR1 in rafts and activating NF-κB signaling to upregulate MMP-1 [29]. Our prior work similarly demonstrated that ACSL4-mediated phospholipid remodeling activates integrin β1 and promotes metastasis in triple-negative breast cancer [25]. In the current study, SHMT2/serine deficiency altered membrane phospholipid composition and fatty acyl chain saturation, leading to reduced membrane fluidity and diminished lipid raft abundance in gastric cancer cells. These biophysical changes impaired CD44 cleavage within rafts and ultimately attenuated GC stemness. Our data thus emphasize the importance of membrane phospholipid remodeling in regulating stemness by modulating the localization and function of key raft-associated proteins such as CD44.

The intracellular domain of CD44 is indispensable for proper membrane trafficking, ligand engagement, and tumor-promoting activity. Mutations or deletions within CD44-ICD cause aberrant surface retention and loss of hyaluronic acid binding, thereby impairing cell motility [30]. CD44-ICD can function independently as a transcriptional regulator or cooperate with partners such as CREB1 to control oncogene expression, including PD-L1 and MMP9 [13, 14]. Here, we establish that CD44-ICD directly drives transcription of the stemness factors KLF4 and c-Myc. Generation of CD44-ICD depends on γ-secretase activity within lipid rafts. Disruption of rafts in circulating tumor cell clusters, for instance, blocks Rac1 signaling and CD44-ICD release, attenuating metastatic potential [31]. Analogously, SHMT2/serine deficiency altered phospholipid composition, mislocalized γ-secretase, and impaired CD44 processing, thereby disrupting stemness maintenance through diminished CD44-

ICD–dependent regulation of KLF4 and c-Myc. While previous reports have linked CD44-ICD to metabolic reprogramming in breast cancer stem cells via PFKFB4 [32], our work highlights the critical interplay between one-carbon metabolism and lipid metabolism orchestrated by SHMT2 in CD44-ICD formation and GCSC stemness control.

Exosomes represent natural nanoscale vehicles capable of transporting diverse therapeutic cargos—including nucleic acids, proteins, and small molecules—while maintaining cargo stability and enabling targeted delivery. For example, exosomal delivery of HGF siRNA has been shown to suppress gastric cancer growth and angiogenesis [33]. Tumor-derived exosomes exploit surface antigen-mediated homologous adhesion for preferential uptake by cancer cells, while HA binding to CD44 further enhances selectivity toward CD44-high cancer stem cells. In this study, we successfully developed HA-modified exosomes loaded with SHMT2 siRNA (HA-Exo-siSHMT2) and confirmed their robust therapeutic activity and favorable safety profile.

Conclusion

In summary, SHMT2, a rate-limiting enzyme in one-carbon metabolism, is markedly upregulated in gastric cancer cells and GCSCs, correlating with aggressive clinicopathological features and poor patient prognosis. Knockdown of SHMT2 decreases serine levels, which triggers remodeling of membrane phospholipids and reduces membrane fluidity, ultimately lowering lipid raft abundance. The resulting impairment in γ-secretase recruitment to rafts inhibits CD44 cleavage and CD44-ICD generation. Consequently, transcriptional activation of c-Myc and KLF4 by CD44-ICD is compromised, leading to disruption of stemness maintenance in gastric cancer. Targeting this axis with HA-Exo-siSHMT2 has demonstrated promising efficacy and safety, supporting its potential as a novel therapeutic strategy for gastric cancer.

Acknowledgments: None

Conflict of Interest: None

Financial Support: None

Ethics Statement: None

References

1. Guo GH, Xie YB, Zhang PJ, Jiang T. Blood index panel for gastric cancer detection. World J Gastrointest Surg. 2022;14(9):1026-36. doi:10.4240/wjgs.v14.i9.1026
2. Eun K, Ham SW, Kim H. Cancer stem cell heterogeneity: Origin and new perspectives on CSC targeting. BMB Rep. 2017;50(3):117-25. doi:10.5483/BMBRep.2017.50.3.222
3. Shen YA, Chen CC, Chen BJ, Wu YT, Juan JR, Chen LY, et al. Potential therapies targeting metabolic pathways in cancer stem cells. Cells. 2021;10(7):1772. doi:10.3390/cells10071772
4. Zhang D, Wang Y, Shi Z, Liu J, Sun P, Hou X, et al. Metabolic reprogramming of cancer-associated fibroblasts by IDH3α downregulation. Cell Rep. 2015;10(8):1335-48. doi:10.1016/j.celrep.2015.02.006
5. Wicks EE, Semenza GL. Hypoxia-inducible factors: Cancer progression and clinical translation. J Clin Invest. 2022;132(11):e159839. doi:10.1172/JCI159839
6. Zhao M, Hou Y, Du YE, Yang L, Qin Y, Peng M, et al. Drosha-independent miR-6778-5p strengthens gastric cancer stem cell stemness via regulation of cytosolic one-carbon folate metabolism. Cancer Lett. 2020;478:8-21. doi:10.1016/j.canlet.2020.02.040
7. Zeng Y, Zhang J, Xu M, Chen F, Zi R, Yue J, et al. Roles of mitochondrial serine hydroxymethyltransferase 2 (SHMT2) in human carcinogenesis. J Cancer. 2021;12(19):5888-94. doi:10.7150/jca.60170
8. Ducker GS, Rabinowitz JD. One-carbon metabolism in health and disease. Cell Metab. 2017;25(1):27-42. doi:10.1016/j.cmet.2016.08.009
9. Muthusamy T, Cordes T, Handzlik MK, You L, Lim EW, Gengatharan J, et al. Serine restriction alters sphingolipid diversity to constrain tumour growth. Nature. 2020;586(7831):790-5. doi:10.1038/s41586-020-2609-x

10. Alecu I, Tedeschi A, Behler N, Wunderling K, Lamberz C, Lauterbach MAR, et al. Localization of 1-deoxysphingolipids to mitochondria induces mitochondrial dysfunction. J Lipid Res. 2017;58(1):42-59. doi:10.1194/jlr.M068676
11. Skandalis SS. CD44 intracellular domain: A long tale of a short tail. Cancers (Basel). 2023;15(20):5041. doi:10.3390/cancers15205041
12. Wöhner B, Li W, Hey S, Drobny A, Werny L, Becker-Pauly C, et al. Proteolysis of CD44 at the cell surface controls a downstream protease network. Front Mol Biosci. 2023;10:1026810. doi:10.3389/fmolb.2023.1026810
13. Kong T, Ahn R, Yang K, Zhu X, Fu Z, Morin G, et al. CD44 promotes PD-L1 expression and its tumor-intrinsic function in breast and lung cancers. Cancer Res. 2020;80(3):444-57. doi:10.1158/0008-5472.CAN-19-1108
14. Miletti-González KE, Murphy K, Kumaran MN, Ravindranath AK, Wernyj RP, Kaur S, et al. Identification of function for CD44 intracytoplasmic domain (CD44-ICD): Modulation of matrix metalloproteinase 9 (MMP-9) transcription via novel promoter response element. J Biol Chem. 2012;287(23):18995-9007. doi:10.1074/jbc.M111.318774
15. Senbanjo LT, Chellaiah MA. CD44: A multifunctional cell surface adhesion receptor is a regulator of progression and metastasis of cancer cells. Front Cell Dev Biol. 2017;5:18. doi:10.3389/fcell.2017.00018
16. Deng J, Ke H. Overcoming the resistance of hepatocellular carcinoma to PD-1/PD-L1 inhibitor and the resultant immunosuppression by CD38 siRNA-loaded extracellular vesicles. Oncoimmunology. 2023;12(1):2152635. doi:10.1080/2162402X.2022.2152635
17. Meng W, He C, Hao Y, Wang L, Li L, Zhu G. Prospects and challenges of extracellular vesicle-based drug delivery system: Considering cell source. Drug Deliv. 2020;27(1):585-98. doi:10.1080/10717544.2020.1748758
18. El-Andaloussi S, Lee Y, Lakhal-Littleton S, Li J, Seow Y, Gardiner C, et al. Exosome-mediated delivery of siRNA in vitro and in vivo. Nat Protoc. 2012;7(12):2112-26. doi:10.1038/nprot.2012.131
19. Aslan C, Maralbashi S, Salari F, Kahroba H, Sigaroodi F, Kazemi T, et al. Tumor-derived exosomes: Implication in angiogenesis and antiangiogenesis cancer therapy. J Cell Physiol. 2019;234(10):16885-903. doi:10.1002/jcp.28374
20. Huang T, Ding X, Xu G, Chen G, Cao Y, Peng C, et al. CDK7 inhibitor THZ1 inhibits MCL1 synthesis and drives cholangiocarcinoma apoptosis in combination with BCL2/BCL-XL inhibitor ABT-263. Cell Death Dis. 2019;10(8):602. doi:10.1038/s41419-019-1831-7
21. Ye Q, Liu Y, Zhang G, Deng H, Wang X, Tuo L, et al. Deficiency of gluconeogenic enzyme PCK1 promotes metabolic-associated fatty liver disease through PI3K/AKT/PDGF axis activation in male mice. Nat Commun. 2023;14(1):1402. doi:10.1038/s41467-023-37142-3
22. Yang L, Hou Y, Du YE, Li Q, Zhou F, Li Y, et al. Mirtronic miR-4646-5p promotes gastric cancer metastasis by regulating ABHD16A and metabolite lysophosphatidylserines. Cell Death Differ. 2021;28(9):2708-27. doi:10.1038/s41418-021-00779-y
23. Xi L, Peng M, Liu S, Liu Y, Wan X, Hou Y, et al. Hypoxia-stimulated ATM activation regulates autophagy-associated exosome release from cancer-associated fibroblasts to promote cancer cell invasion. J Extracell Vesicles. 2021;10(11):e12146. doi:10.1002/jev2.12146
24. McBride MJ, Hunter CJ, Zhang Z, TeSlaa T, Xu X, Ducker GS, et al. Glycine homeostasis requires reverse SHMT flux. Cell Metab. 2024;36(1):103-15.e4. doi:10.1016/j.cmet.2023.12.001
25. Qiu Y, Wang X, Sun Y, Jin T, Tang R, Zhou X, et al. ACSL4-mediated membrane phospholipid remodeling induces integrin β1 activation to facilitate triple-negative breast cancer metastasis. Cancer Res. 2024;84(11):1856-71. doi:10.1158/0008-5472.CAN-23-2491
26. Choi YJ, Lee G, Yun SH, Lee W, Yu J, Kim SK, et al. The role of SHMT2 in modulating lipid metabolism in hepatocytes via glycine-mediated mTOR activation. Amino Acids. 2022;54(5):823-34. doi:10.1007/s00726-022-03141-9
27. Ghrayeb A, Finney AC, Agranovich B, Peled D, Anand SK, McKinney MP, et al. Serine synthesis via reversed SHMT2 activity drives glycine depletion and acetaminophen hepatotoxicity in MASLD. Cell Metab. 2024;36(1):116-29.e7. doi:10.1016/j.cmet.2023.12.013

28. Bi J, Ichu TA, Zanca C, Yang H, Zhang W, Gu Y, et al. Oncogene amplification in growth factor signaling pathways renders cancers dependent on membrane lipid remodeling. Cell Metab. 2019;30(3):525-38.e8. doi:10.1016/j.cmet.2019.06.014
29. Yang YF, Jan YH, Liu YP, Yang CJ, Su CY, Chang YC, et al. Squalene synthase induces tumor necrosis factor receptor 1 enrichment in lipid rafts to promote lung cancer metastasis. Am J Respir Crit Care Med. 2014;190(6):675-87. doi:10.1164/rccm.201404-0714OC
30. Jou IM, Wu TT, Hsu CC, Yang CC, Huang JS, Tu YK, et al. High molecular weight form of hyaluronic acid reduces neuroinflammatory response in injured sciatic nerve via the intracellular domain of CD44. J Biomed Mater Res B Appl Biomater. 2021;109(5):673-80. doi:10.1002/jbm.b.34731
31. Li D, Park Y, Hemati H, Liu X. Cell aggregation activates small GTPase Rac1 and induces CD44 cleavage by maintaining lipid raft integrity. J Biol Chem. 2023;299(12):105377. doi:10.1016/j.jbc.2023.105377
32. Gao R, Li D, Xun J, Zhou W, Li J, Wang J, et al. CD44ICD promotes breast cancer stemness via PFKFB4-mediated glucose metabolism. Theranostics. 2018;8(22):6248-62. doi:10.7150/thno.28721
33. Zhang H, Wang Y, Bai M, Wang J, Zhu K, Liu R, et al. Exosomes serve as nanoparticles to suppress tumor growth and angiogenesis in gastric cancer by delivering hepatocyte growth factor siRNA. Cancer Sci. 2018;109(3):629-41. doi:10.1111/cas.13488